



Published in final edited form as:

Structure. 2018 November 06; 26(11): 1431–1439.e6. doi:10.1016/j.str.2018.07.007.

Chemical crosslinking mass spectrometry reveals the conformational landscape of the activation helix of PPAR γ ; a model for ligand-dependent antagonism

Jie Zheng^{#1}, Cesar Corzo^{#1}, Mi Ra Chang¹, Jinsai Shang², Vinh Q. Lam¹, Richard Brust², Anne-Laure Blayo¹, John B. Bruning³, Theodore M. Kamenecka¹, Douglas J. Kojetin^{1,2}, and Patrick R. Griffin^{1,2,*}

¹The Scripps Research Institute, Department of Molecular Medicine, Jupiter, FL 33458, USA

²Department of Integrative Structural and Computational Biology, The Scripps Research Institute, Jupiter, Florida 33458, USA

³The University of Adelaide, Institute for Photonics & Advanced Sensing (IPAS), School of Biological Sciences, University of Adelaide, Adelaide, SA 5005, Australia

These authors contributed equally to this work.

Summary

Peroxisome proliferator-activated receptors (PPARs) are pharmacological targets for the treatment of metabolic disorders. Previously, we demonstrated the antidiabetic effects of SR1664, a PPAR γ modulator lacking classical transcriptional agonism, despite its poor pharmacokinetic properties. Here we report identification of the antagonist SR11023 as a potent insulin sensitizer with significant plasma exposure following oral administration in mice. To determine the structural mechanism of ligand-dependent antagonism of PPAR γ , we employed an integrated approach combining solution-phase biophysical techniques to monitor activation helix (helix 12) conformational dynamics. While informative on receptor dynamics, HDX-MS and NMR data provide limited information regarding the specific orientations of structural elements. In contrast, label free quantitative crosslinking mass spectrometry (XL-MS) revealed that binding of SR11023 to PPAR γ enhances interaction with co-repressor motifs by pushing H12 away from the agonist active conformation towards the H2-H3 loop region (i.e., the omega loop), revealing the molecular mechanism for active antagonism of PPAR γ .

*To whom correspondence could be addressed: Lead Contact: pgriffin@scripps.edu.

AUTHOR CONTRIBUTIONS

Conceptualization, Z.J., C.C. and P.R.G.; Methodology, M.R.C., V.Q.L., R.B., A.L.B performed and supported experimental assays and animal studies. J.S and D.J.K performed and analyzed NMR data. J.B.B performed molecular docking experiment. T.M.K performed SAR studies of SR11023. J.Z. and P.R.G. performed XL-MS studies. Writing – Review & Editing, J.Z., C.C., D.J.K. and P.R.G.; Supervision, P.R.G.

DECLARATION OF INTERESTS:T.M.K. and P.R.G. have WO2012170561 – US2012/0309769 patent for SR11023 reported in this manuscript.

INTRODUCTION

Peroxisome proliferator-activated receptor gamma (PPAR γ), a member of the nuclear receptor superfamily of transcriptional factors, has been implicated in type 2 diabetes, a disease characterized by a state of insulin resistance and glucose intolerance. PPAR γ is the pharmacological target of the thiazolidinedione (TZD) class of antidiabetic drugs, including rosiglitazone and pioglitazone (Mayans, 2015; Wright et al., 2014). However, treatment of type 2 diabetes mellitus (T2DM) has moved away from administration of TZDs as safety concerns over their use has grown. While weight gain is associated with use of TZDs, the major safety concerns include edema, plasma volume expansion that is linked to cardiomegaly and heart failure, increased risk of bone fractures, and a slight increased risk for bladder cancer (specific to pioglitazone) (Kung and Henry, 2012; Rubenstrunk et al., 2007; Shi et al., 2011). As an attempt to dissociate efficacy from side effects, selective PPAR γ partial agonist termed SPPAR γ M were developed that exhibit significantly reduced receptor target gene expression without loss of anti-diabetic efficacy in rodent models of T2DM (Liu et al., 2005; Minoura et al., 2004). For example, MRL24, a potent PPAR γ partial agonist, was shown to be anti-diabetic in *db/db* mice with no detectable cardiac hypertrophy, minimal increases in plasma volume, and no increase in extracellular fluid volume (Acton et al., 2009; Acton et al., 2005). Subsequent studies were conducted to examine this mechanism of action for both agonists and partial agonists. These studies demonstrated that the insulin sensitization afforded by partial agonist and TZD agonist treatment tightly correlate with the ability of these drugs to block the obesity-induced phosphorylation of PPAR γ at S273 (pS273) (Choi et al., 2010). This work was followed by demonstration that the PPAR γ antagonist SR1664, a compound that potently blocks pS273 but does not increase expression of pro-adipogenic PPAR γ target genes, was an efficacious insulin sensitizer in rodent models of diabetes (Choi et al., 2011). Unfortunately, SR1664 suffers from poor pharmacokinetic properties thus limiting its utility in chronic studies. To improve the pharmaceutical properties of SR1664, extensive SAR studies were carried out (Asteian et al., 2015). Here, we report that the optimized SR1664 analog SR11023 demonstrates significantly improved pharmacokinetic properties such that the compound can be administered orally at relatively low doses resulting in substantial drug levels in blood and white adipose tissue (WAT), the metabolic tissue where PPAR γ activity is critical for systemic insulin sensitivity (Kintscher and Law, 2005; Sugii et al., 2009).

To assist the SAR studies, we sought to understand the structural basis for antagonism of PPAR γ by probing the receptor global and local dynamics in the context of ligand binding, co-activator and co-repressor NR box motif recruitment. The C-terminal most helix of most NRs, H12 or activation helix (AH or AF2), is often described as the molecular switch governing the transitions between active and inactive conformations (Heldring et al., 2007). Binding of agonist ligands to the NR ligand binding pocket shifts H12 towards an active conformation to facilitate recruitment of transcriptional coactivators (e.g., p160 family members such as SRC1) that tether histone acylation activity relaxing chromatin allowing RNA polymerase II binding to the target gene. In contrast, repressive ligands (antagonists and inverse agonists) shift H12 towards an inactive conformation facilitating receptor interaction with co-repressor proteins such as N-CoR (nuclear receptor corepressor) or

SMRT (silencing mediator for retinoid and thyroid hormone receptors). These corepressor proteins tether histone deacetylases to the transcriptional complex to promote condensation of chromatin to shut down transcription (Horlein et al., 1995; Hu and Lazar, 1999; Nagy et al., 1999). The receptor interaction domain (RID) of these coregulatory proteins contain highly conserved hydrophobic helical motifs called NR boxes that engage the region of H12 referred to as AF2 (activation function 2). The RID of coactivator proteins contain 5' - LXXLL - 3' motifs whereas corepressor proteins contain 5' - LXXI/HIXXXL/I - 3' motifs called CoRNR boxes (Xu et al., 2002b). While high resolution atomic structures exist for most ligand binding domains (LBD) of NRs, the orientation of H12 upon binding to repressive ligands and NR or CoRNR box peptides most often is not resolved by co-crystallography. To address this shortcoming, we employed an integrated approach using solution based techniques — chemical crosslinking mass spectrometry (XL-MS), hydrogen/deuterium exchange mass spectrometry (HDX-MS) and nuclear magnetic resonance (NMR) spectroscopy — to aid structural characterization of ligand binding-mediated coactivator/corepressor receptor interactions and H12 dynamics. XL-MS has been used to gain insights into structural rearrangement between protein subunits (Wu et al., 2013), protein conformational changes (Schmidt and Robinson, 2014), and the assembly of large protein complexes (Chen et al., 2010; Knutson et al., 2014). We demonstrate that SR11023 is a potent antagonist of PPAR γ with strikingly improved pharmacokinetics over SR1664, blocks pS273 and lacks classic agonist properties. Unlike full agonist TZDs, binding of SR11023 to PPAR γ only results in stabilization of H3. This is in accordance with a molecular docking model that unlike full and partial agonists, SR11023 adopts a distinct conformation residing beside H3 and facing away from AF2 surface. Solution based biophysical analyses further reveal that H12 does in fact act as a molecular switch governing the ligand-dependent activation of PPAR γ . Instead of being trapped in one conformation as observed in numerous co-crystallographic studies, H12 possesses structural dynamics in solution and adopts unique ensembles of conformers depending on the receptor/ligand/NR-box peptide complex. Binding of SR11023 enhances the receptor interaction with co-repressor motifs by driving H12 away from agonist position towards the H2-H3 loop region (omega loop) of the protein. These results suggest a unique yet to be observed molecular mechanism for SR11023-mediated antagonism of PPAR γ .

RESULTS

Pharmacological antagonism of PPAR γ by SR11023:

The poor pharmacokinetic (PK) properties of SR1664 restricted its route of drug administration to intraperitoneal injection. Efforts to improve the PK properties and to develop SAR around the core biaryl indole scaffold of SR1664 led to the synthesis of a wide range of analogs. Compounds were screened in cell-based assays to identify compounds that exhibit minimal PPAR γ transactivation activity (<10% at 1 μ M in Gal4-LBD assays and ~0% in full length PPRE assays) while retaining good binding affinity to PPAR γ (IC₅₀ < 250 nM in a competitive displacement assay). Compounds that met these criteria were evaluated in rodent PK studies to identify analogs that exhibited excellent plasma exposure following oral administration. Previously it has been demonstrated that the substitution of t-butyl for nitro at the para position of SR1664 led to identification of a series of inverse

agonists (e.g., SR2595 and SR10171) that suppress receptor basal transcriptional activity; and although SR2595 and SR10171 exhibit beneficial effects on osteogenesis in multipotent mesenchymal stem cells (MSCs) and bone metabolism in mouse models, these compounds repress PPAR γ target gene expression suggesting different mechanism from the antagonist SR1664 (Marciano et al., 2015; Stechschulte et al., 2016). Further optimization of the SR1664 scaffold, including substitution of cyclopropane for trifluoromethyl at the meta position of the left-hand benzyl group, resulted in identification of the antagonist SR11023 which exhibited good binding affinity ($IC_{50} = 108\text{nM}$) yet poor transactivation activity in the GAL4-PPARG assay ($2.7\mu\text{M}$, 10% Max.Stim), similar to that observed for SR1664 ($4.5\mu\text{M}$, 10% Max.Stim) (Table 1). Note that poor transactivation is not due to lack of cell penetration as both SR1664 and SR11023 significantly right-shift the dose response curve for rosiglitazone in the GAL4-PPARG assay (data not shown). In addition, in both human PPAR α (hPPAR α) and hPPAR δ -Gal4 transactivation assays, SR11023 and rosiglitazone exhibited no transcriptional agonism (Figure S1A).

As previously shown, the insulin sensitization efficacy of antagonist ligands such as SR1664, correlates with their ability to reduce phosphorylation of PPAR γ at S273 (pS273) (Choi et al., 2011). In an *in vitro* kinase assay, dose-dependent reduction in pS273 was observed for the SR11023 treated receptor (25% at $2\mu\text{M}$ and 75% at $20\mu\text{M}$) as compared to DMSO only controls. This result suggested that SR11023 can reduce pS273 and should demonstrate antidiabetic properties in rodents (Table 1 and Figure S1B). Unlike rosiglitazone and similar to SR1664, SR11023 possesses minimal adipogenic activity in differentiated 3T3-L1 cells as demonstrated by the absence of lipid formation and lack of upregulation of the PPAR γ -driven pro-adipogenic genes, e.g. aP2 and cd36 (Figure 1A and Figure 1B). To obtain an unbiased assessment of the compounds' impact on gene expression in adipocytes, we performed RNA-seq of mRNA isolated from 3T3-L1 cells incubated with rosiglitazone, SR11023, or DMSO-only for 6 days. Rosiglitazone exhibited robust activation of a large gene set containing many known PPAR γ target genes whereas SR11023 displayed very modest regulation of only a small subset of PPAR γ controlled genes (Figure 1C), reminiscent of that observed for the antagonist SR1664 (Choi et al., 2011). However, unlike SR1664, SR11023 showed significant plasma exposure in C57BL/6 mice following oral administration; two hours after dosing either both compound at $40\text{mg}\cdot\text{kg}^{-1}$, the plasma concentration of SR11023 reached $70\mu\text{M}$ whereas SR1664 plasma exposure was less than $1\mu\text{M}$ (Figure S1C). Thus, SR11023 is a potent antagonist of PPAR γ with strikingly improved pharmacokinetics over SR1664, blocks pS273 and lacks classic agonist properties.

SR11023 has a distinct binding mode within PPAR γ and enhances interaction with co-repressor peptides:

Next, we applied molecular docking, HDX-MS, and NMR to investigate SR11023 interactions with receptor. Using *in silico* docking, superimposition of SR11023 with the binding poses for rosiglitazone (PDB:1PRG) and the partial agonist MRL24 (PDB:2Q5P) within the ligand binding pocket (LBP) of PPAR γ suggests that SR11023 adopts a relatively linear orientation facing away from the AF2 surface residing along H3. In contrast, both rosiglitazone and MRL24 display curved shaped conformations with the thiazolidinedione of rosiglitazone and the indole of MRL24 oriented towards AF2 surface. These distinct

orientations within the LBP are consistent with results from HDX-MS analyses that reveal the exchange kinetics of the H11-H12 region of PPAR γ was insensitive to SR11023 binding whereas rosiglitazone, and MRL24 to a lesser extent, stabilize the C-terminal end of H11 and H11-H12 loop region as demonstrated by reduced solvent exchange (Figure 1E and Figure S2A). Only binding of rosiglitazone to PPAR γ results in full stabilization of H12 (Figure 1E and Figure S2A). Among these ligands, NMR analysis reveals that a NMR peak corresponding to Y473, which resides on H12, is only present for rosiglitazone, indicating H12 is dynamic on the μ s-ms time scale in the *apo* form or when bound to MRL24 or SR11023 (Figure S2B). Binding of all three ligands to PPAR γ afforded strong protection to solvent exchange in H3, residues 279–286 and 287–298, further supporting that SR11023 possesses high binding affinity with receptor comparable to that of rosiglitazone and MRL24 (Figure 1E and Figure S2A). In a TR-FRET peptide interaction assay, both rosiglitazone and MRL24 enhanced the association of PPAR γ with NR box peptides derived from the coactivators p300 and SRC1 (SRC1–2), whereas in the presence of SR11023, there was no enhanced interaction. In contrast, in the presence of SR11023, receptor interaction with peptides derived from the corepressors NCOR1 (NCOR1–3) and SMRT (SMRT-2) was increased whereas binding of either rosiglitazone or MRL24 facilitated dissociation of these corepressor peptides (referred to as CoRNR box peptides) from PPAR γ (Figure 1F).

XL-MS reveals mobility of PPAR γ H12 influenced by SR11023 and corepressor peptide:

The structural switch of H12 in the LBD of NRs between an inactive towards an active conformation is considered a classical model of AF2 ligand-dependent activation (Heldring et al., 2007; le Maire et al., 2010). However, the orientation of H12 of PPAR γ in non-active conformations is hard to resolve. Co-crystallography of *apo* and ligand bound LBD all reveal H12 in an active conformation (Bruning et al., 2007). Previous studies using HDX-MS and NMR have shown that the dynamics of H12 are differentially altered by ligands. However, these techniques, which examine receptor hydrogen bond networks and changes in chemical environment via chemical shift perturbations, do not provide insight into the structural orientation of H12. To address this, we applied label free quantitative crosslinking mass spectrometry to examine the solution state mobility of PPAR γ H12 in the presence and absence of ligands, co-activator and or co-repressor peptides. XL-MS studies were performed with the BS3 crosslinker where two proximal lysine residues within the distance of \sim 24 Å can be crosslinked (6 Å side chain of each lysine and the 11.4 Å spacer of BS3). In several published studies, a distance range of 25–30 Å is considered as a reasonable crosslink limit, measured between alpha-carbon atoms of lysine (a tolerance about 3 Å is added to the theoretical maximum cross-linking distance of BS3) (Fischer et al., 2013; Merkley et al., 2014). A summary of identified XL peptides is shown in Table S1. XL-MS studies of *apo* PPAR γ demonstrated that lysine474 (K474) which is part of a H12 peptide, **K(474)DLY**, was capable of forming crosslinks between several lysines including **LQVIK(457)K** (part of H11), **AK(301)SIPGF** (C-terminal region of H3), **QEQSK(265)EVAIR** and **FK(275)HITPL** (part of the H2-H3 loop). The MS/MS spectra of these XL peptides are shown in Figure S3. The ion intensities and peak areas of these crosslinked peptides in twenty different experimental conditions (3 replicates each condition) were manually calculated and compared. The results from this analysis are displayed in Figure 2. The highest peak intensity (derived from selected ion chromatograms

(SICs)) across twenty XL samples (including 3 replicates) in each peptide panel - SVEAVQEITEY +2, K224-K232 XL peptide, K474-K457 XL peptide, K474-K257 XL peptide, K474-K265 XL peptide and K474-K301 XL peptide - were normalized as 100% bar plot. For all other peptides, their rest peak abundances within an indicated peptide panel were scaled accordingly. The intensity of the peptide that contains K224-K232 conjugation between H1-H2 was used as an internal control since this region of the receptor is not involved in ligand or NR box peptide binding. As expected, similar signal intensity was observed for this peptide in all conditions. An additional internal control was peptide SVEAVQEITEY (634.31 m/z, +2) which lacks a lysine residue and thus cannot be conjugated with BS3, afforded similar peak intensity across all samples (Figure 2A and B). These crosslinking results displayed in Figure 2 suggest that H12 of *apo* receptor is a dynamic ensemble of distinct conformers. This observation is in contrast to the locked conformation of H12 observed in the crystal structure of *apo* PPAR γ (Bruning et al., 2007).

The conformational dynamics of the activation helix of PPAR γ (H12) is influenced upon receptor binding to pharmaceutically distinct ligands and or sequence specific NR or CoRNR box peptides. The higher the MS signal intensity of a particular crosslinked peptide pair that includes conjugation between H12 and one distal lysine within PPAR γ , the more the population of H12 conformers are orientated towards that lysine residue. On the other hand, the lower the MS signal intensity, that conformer is less populated. Label free quantitative XL-MS studies of PPAR γ LBD in the presence of either rosiglitazone, MRL24, or SR11023 resulted in changes in the peak intensities of various crosslinked peptides as compared to those observed for *apo* receptor. As shown in Figure 2C, addition of the co-activator SRC1-2 NR box peptide to either *apo* receptor or ligand bound receptor selectively increased the abundance of the intensity of ions corresponding to the crosslink between K457-K474, suggesting that co-activator peptide binding drives increased populations of H12 towards H11 K457 residue. In the reported X-ray crystal structure, coactivator peptide binding reinforces H12 docking against H11 (Nolte et al., 1998). Although crosslinks between K474-K457 and K474-K301 were observed in the presence of all ligands, agonist and SRC1-2 binding afforded a statistically significant reduction in the intensity (population) of K474-K265 and K474-K275 crosslinks, suggesting that H12 in the agonist complex cannot effectively sample the longer-distance conformers; K474 to K275 at ~ 26 Å and K474 to K265 at ~ 35 Å (determined from PPAR γ X-ray structure PDB: 2PRG) (Figure 2D and E). In contrast, SR11023 binding to receptor restored these longer distance crosslinks as represented by an increased intensity of K474-K275 and K474-K265 XL peptides (Figure 2D and E). Similar intensities of ions corresponding to crosslinks for K474-K265 and K474-K275 were observed in when comparing PPAR γ alone (homodimer) or PPAR γ /RXR α heterodimer, suggesting that these crosslinks are intra-molecular and not inter-molecular (Figure 2 and Figure S4). These data demonstrate that the mobility of H12 in the *apo* receptor is reduced upon ligand binding and that H12 adopts different orientations relative to AF2 when comparing agonist to antagonist bound receptor (Figure 3). The largest change in peak intensities for crosslinks was mediated by antagonist bound receptor in the presence of the co-repressor peptide NCOR1-3 (Figure 2F). In this experiment, the crosslink between K474-K301 was abrogated while the intensity of crosslinks between K474-K265/

K275 increased with statistical significance, suggesting a stable re-orientation of H12 in proximity of H2-H3 loop region (Figure 2 D, E, F and Figure 3).

NMR and HDX-MS data provide complimentary information to the XL-MS data:

Further evidence for corepressor binding affecting the K474-K301 structural perturbation was obtained by protein NMR, which revealed that addition of NCOR1–3 or SMRT2 peptide caused NMR chemical shift perturbations for residues within the AF-2 surface, including the site of crosslinking (K301) and other nearby residues (e.g., I303 and V307) (Figure 4A). Combined with the crosslinking data, these results indicating that binding of the co-repressor peptides, which have nearly identical affinity for PPAR γ (Figure 4B), to this region can block BS3 crosslinks at K301. Although NCOR1–3 and SMRT-2 share a conserved CoRNR box motif 5' – LXXI/HIXXXL/I – 3', SMRT-2 was not as efficient as NCOR1–3 at altering H12 orientation (Figure 2). Additionally, HDX-MS analysis revealed that NCOR1–3, when bound to *apo* PPAR γ , destabilized H12 to a greater extent than SMRT-2 (Figure S2A). It is likely that the NCOR1–3 peptide docks into the AF2 hydrophobic cleft in a slightly different orientation than the SMRT-2 peptide, which is supported by the NMR results showing differences in the peptide-bound peaks for residues in this region, resulting in enhanced ability to disrupt the charge-clamp within the AF2 surface. In general, the observations described above are consistent with the reported crystal structures of co-repressor and antagonist bound RAR LBD and PPAR α LBD wherein NCOR or SMRT peptide binding occupies the H3-H5 binding groove within the AF2 surface and displaces AF2 helix from folding back to the agonist position (le Maire et al., 2010; Xu et al., 2002a). Taken together, differences in compound structure and the specific NR-box sequence combine to impact the mobility of AF2, which in turn impacts PPAR γ transcriptional activity. Binding of SR11023 to PPAR γ would blunt activation of its target genes by maintaining co-repressor interaction and keeping the receptor in an inactive conformation.

DISCUSSION

The TZD class of drugs function as full agonists of PPAR γ and have been used to treat T2DM. However, their diminished clinical usage due to undesirable side effects has given rise to the necessity to develop the next generation of class of insulin sensitizers that afford dissociation of classical agonism (Rizos et al., 2009). The antidiabetic actions of rosiglitazone and MRL24 have been shown to tightly correlate with their abilities to block PPAR γ pS273, where the degree of phosphorylation at this site is associated with obesity and impaired glucose tolerance (Banks et al., 2015; Choi et al., 2010). The discovery of SR1664 proved a therapeutic concept that it is possible to develop a PPAR γ ligand blocking pS273 that is devoid of classical agonism, yet retains TZD-like antidiabetic activities in animal models (Choi et al., 2011). In this study, we profile a PPAR γ modulator SR11023 that possesses therapeutic potential for treatment of T2DM. We show that SR11023 exhibits the ability to block pS273 yet has significantly improved pharmacokinetic properties compared to that of SR1664. Yet unlike TZDs, SR11023 is absent of pro-adipogenic behavior and lacks the classical agonism to upregulate PPAR γ target gene expressions in 3T3-L1 cells.

We investigated the structural determinants of SR11023 mediated PPAR γ inactivation and examined the role of H12 as a molecular switch governing ligand-dependent activation of PPAR γ . Unlike TZDs, binding of SR11023 to PPAR γ only results in stabilization of H3. This is in accordance with molecular docking model that unlike full and partial agonists, SR11023 adopts distinct conformation residing beside H3 and facing away from AF2 surface. While HDX-MS and NMR data provide molecular hydrogen bonding activities and chemical perturbations, both of them yield limited information regarding orientation of concrete structural elements. XL-MS provides an orthogonal approach to detect the mobility of H12 with respect to residue-residue distance, residue solvent exposure, and local conformational rearrangement. Label free quantitative XL-MS was used to profile four distinct H12 helix crosslinking reactions in 20 different protein states. One advantage of label free quantitation is that there are no limits to the number of samples that can be compared. In one study, the robustness and reproducibility of this quantitation method has been examined (Muller et al., 2018). Instead of being trapped in one conformation as observed in numerous co-crystallographic studies, H12 possesses structural dynamics in aqueous environment and its conformational landscape can vary in a ligand and coregulator dependent manner. For example, rosiglitazone binding to receptor blocks H12 from conjugation to H2-H3 loop region, yet these long-range crosslinks are restored when the receptor is bound to SR11023. GW9662, a potent covalent antagonist, drives H12 populations to K265 region nearly two times more than that observed with the reversible antagonist SR11023, further indicating the greater potency of GW9662 to drive the largest degree of H12 mobility. In addition, sequence specific NR-box peptides play a potential role in regulation of H12 conformational mobility. Co-activator peptide binding reinforces AF2 helix docking against H11 whereas co-repressor peptide binding displaces AF2 helix from folding back to the agonist position. HDX-MS shows that NCOR1–3 exhibits enhanced ability to allosterically destabilize C-terminal H11 and H12 region in *apo* receptor compared to that observed with SMRT-2 peptide. Correspondingly, the presence of NCOR1–3 drives higher conformational population of H12 proximal to H2-H3 loop region, suggesting the differential regulatory roles of NCOR1–3 and SMRT-2. Combined, these data suggest that binding of SR11023 enhances the receptor interaction with co-repressor motifs by driving resulting H12 away from the agonist position towards H2-H3 loop region to avoid clashing. This observation suggests a molecular mechanism for SR11023-mediated antagonism of PPAR γ .

STAR METHODS

KEY RESOURCES TABLE

REAGENT or RESOURCE	SOURCE	IDENTIFIER
Antibodies		
LanthaScreen Elite Tb-anti-His Antibody	Thermo Fisher Scientific	Cat:PV5863
LanthaScreen Tb-anti-GST-antibody	Thermo Fisher Scientific	Cat:PV3550
Bacterial and Virus Strains		
BL21(DE3) E. coli cells	New England Biolabs	Cat:C2527
Biological Samples		
HEK293T	ATCC	Cat:CRL-3216

REAGENT or RESOURCE	SOURCE	IDENTIFIER
3T3-L1 fibroblasts	ATCC	Cat:CL-173
Chemicals, Peptides, and Recombinant Proteins		
9-cis Retinoic Acid	Cayman Chemical	Cat:14587
Ammonium Chloride, 99% ¹⁵ N	Cambridge Isotope Labs	Cat:NLM-467
Deuterium Oxide, 99.9% D	Sigma-Aldrich	Cat:151882
Dimethyl Sulfoxide-d ₆ , 99.9% D	Cambridge Isotope Labs	Cat:DLM-10
Fluorescein Isothiocyanate Isomer I	Sigma-Aldrich	Cat:4274
HiLoad 16/600 Superdex 75 pg column	GE Healthcare Life Sciences	Cat:28989333
HiLoad 16/600 Superdex 200 pg column	GE Healthcare Life Sciences	Cat:28989335
HisTrap HP Ni NTA column	GE Healthcare Life Sciences	Cat:17-5248-02
Hypersil GOLD C8 LC column	Thermo Fisher Scientific	Cat:25205
Hypersil GOLD C18 LC column	Thermo Fisher Scientific	Cat:25012
Oil Red dye	Sigma-Aldrich	Cat:O0625
Rosiglitazone	Sigma-Aldrich	Cat:R2408
SR11023	Made by T.M.K.	Patent: WO2012170561 – US2012/0303769
GST-PPAR γ -LBD	Thermo Fisher Scientific	Cat:PV4545
GST-PPAR α -LBD	Thermo Fisher Scientific	Cat:PV4691
Cdk5/p35 kinase	Milipore	Cat: 14-477
Fluormone Pan-PPAR Green	Thermo Fisher Scientific	Cat:PV4896
3-iso-butyl-1-methylxanthine	Sigma-Aldrich	Cat:I7018
Dexamethasone	Sigma-Aldrich	Cat:D4902
Insulin	Sigma-Aldrich	Cat:I9278
X-treme Gene 9 transfection reagent	Sigma-Aldrich	Cat: 6365779001
SYBR green fluorescent dye	Bio-Rad	Cat: 1725271
TR-FRET Nuclear receptor buffer F	Thermo Fisher Scientific	Cat: PV4547
Pepsin column	(Busby et al., 2007)	http://www.sciencedirect.com/science/article/pii/S1387380600404040
C8 trap column, 1 mm x 10 mm	Thermo Scientific	Cat:25205-011001
Betasil C8 column, 5 μ 10x1 mm	Thermo Scientific	Cat:25203-051030
DTT	Sigma	Cat:10708984001
Iodoacetamide	Sigma	Cat:I1149
Trypsin	Promega	Cat:V5111
FITC-NH-ASKHKQLSELLRSGSS	LifeTein, LLC	N/A
FITC-NH-TNMGLEAIIRKALMGKYDQWEE	LifeTein, LLC	N/A
FITC-NH-LTERHKILHRLLEQEGSPSD	LifeTein, LLC	N/A
FITC-NH-ASNLGLEIIRKALMGSPD	LifeTein, LLC	N/A
NH-ASKHKQLSELLRSGSS	LifeTein, LLC	N/A
NH-TNMGLEAIIRKALMGKYDQWEE	LifeTein, LLC	N/A
NH-LTERHKILHRLLEQEGSPSD	LifeTein, LLC	N/A
NH-ASNLGLEIIRKALMGSPD	LifeTein, LLC	N/A
Spectra Multicolor Broad Range Protein Ladder	Thermo Fisher Scientific	Cat:26634
BS3 crosslinker	Thermo Fisher Scientific	Cat:21580
Chymotrypsin	Promega	Cat:V1061
Human PPAR γ LBD, residues 231-505; isoform 2	(Hughes et al., 2012)	N/A
Human RXR α LBD, residues 223-462	(Kojetin et al., 2015)	N/A
PPAR γ LBD crystal structure	(Nolte et al., 1998)	PDB code: 2PRG
Critical Commercial Assays		

REAGENT or RESOURCE	SOURCE	IDENTIFIER
Qiazol reagent	Qiagen	Cat:79306
RNeasy Mini Kit	Qiagen	Cat:74104
LanthaScreen TR-FRET PPAR γ competitive binding assay kit	Thermo Fisher Scientific	Cat:PV4893
High Capacity Reverse Transcription Kit	Applied Biosystems	Cat:4368814
HTScan CDK/Cyc kinase assay kit	Cell Signaling Technology	Cat:7519
RNeasy Mini Kit	Qiagen	Cat:74106
TruSeq stranded mRNA sample prep protocol	Illumina	Cat:RS-122-2101
Experimental Models: Cell Lines		
HEK293T	ATCC	Cat:CRL-3216
3T3-L1 fibroblasts	ATCC	Cat:CL-173
Software and Algorithms		
HDX Workbench	(Pascal et al., 2012)	http://hdxworkbench.com
Mascot	Matrix Science	http://www.matrixscience.com/
Plink2	Pfind Studio (Yang et al., 2012)	http://pfind.ict.ac.cn/software/pLink1/index.html
Deposited mass spectrometry raw data		
XL-MS data	PRIDE (https://www.ebi.ac.uk/pride/archive/)	Accession number: PXD010222
HDX-MS data	Figshare (https://figshare.com)	https://figshare.com/s/d9fe41df3e945828e548
Other		
Q Exactive Mass spectrometer	Thermo Fisher Scientific	Cat:IQLAAEGAAPPALGMAZR

CONTACT FOR REAGENT AND RESOURCE SHARING

Further information and requests for resources and reagents should be directed to and will be fulfilled by the Lead Contact PRG (pgriffin@scripps.edu).

EXPERIMENTAL MODEL AND SUBJECT DETAILS

The species/strain of experimental models of HEK293T cells are female Homo sapiens embryonic kidney 293 cells contains the SV40 T-antigen. HEK293T cells were cultured with Duplecco's Modified Eagle's Medium (DMEM) contained 10% Fetal Bovine Serum (heat inactivated), 2mM L-glutamine, 1% Penicillin/Streptomycin in 37°C, 5% CO₂ incubator. The authentication of cell lines is ATCC (Cat: CRL-3216). The species/strain of experimental models of 3T3-L1 fibroblasts cells are male Mus musculus embryo fibroblasts. 3T3-L1 cells were cultured with Duplecco's Modified Eagle's Medium (DMEM) contained 10% Fetal Bovine Serum (heat inactivated), 2mM L-glutamine, 1% Penicillin/Streptomycin in 37°C, 5% CO₂ incubator. The authentication of cell lines is ATCC (Cat: CL-173).

METHOD DETAILS

Synthesis of SR11023 method: (S)-2-(4-((5-((1-(3-cyclopropylphenyl)ethyl)carbonyl)-2,3-dimethyl-1H-indol-1-yl)methyl)phenyl)-2-methylpropanoic acid. Commercially available 2,3-dimethyl-1H-indole-5-carboxylic acid was N-alkylated with commercially available methyl 2-(4-(bromomethyl)phenyl)-2-methylpropanoate using NaH in DMF. The resulting acid was subsequently coupled with (S)-1-(3-cyclopropylphenyl) ethanamine using 2-(3H-[1,2,3]triazolo[4,5-b]pyridin-3-yl)-1,1,3,3-tetramethylisouronium hexafluorophosphate(V) (HATU) and diisopropylethylamine in CH₂Cl₂ to provide the amide. The methyl ester was finally

hydrolysed using aqueous NaOH in ethanol to give the crude acid which was purified by flash chromatography (ethyl acetate/hexanes 10–100%) to give the title compound as a colorless solid. Electrospray ionization coupled with mass spectrometry (ESI-MS; m/z): 509.27 [M+H]⁺; ¹H NMR (400 MHz, dimethylsulphoxide (DMSO)-d₆): δ (p.p.m.) δ 12.34 (broad s, 1H), 8.63 (d, 1H, J=8.0 Hz), 8.12 (d, 1H, J=1.2 Hz), 7.65 (dd, 1H, J=8.4 Hz, 1.6 Hz), 7.44 (d, 1H, J=8.8 Hz), 7.28 (d, 1H, J=8.8 Hz), 7.24–7.18 (m, 4H), 6.97–6.92 (m, 3H), 5.43 (s, 2H), 5.20 (q, 1H, J=7.2 Hz), 2.54 (q, 2H, J=1.6 Hz), 2.33 (s, 2H), 2.30 (s, 2H), 1.95–1.92 (m, 1H), 1.51 (d, 3H, J=7.6 Hz), 1.44 (s, 6H), 0.97–0.95 (m, 2H), 0.69–0.67 (m, 2H); ¹³C NMR (100 MHz, d-DMSO) 177.82, 166.51, 145.26, 144.01, 143.40, 137.49, 136.44, 133.92, 128.06, 127.51, 125.96, 125.86 (2C), 125.17 (2C), 123.45, 123.14, 123.07, 120.24, 117.59, 108.64, 107.12, 48.24, 45.51, 45.49, 26.30, 22.42, 15.09 (2C), 10.00, 9.27 (2C), 8.72.

Differentiation of 3T3-L1 cells—was induced with a cocktail consisting of 0.5 μ M 3-isobutyl-1-methylxanthine (Cat: I7018), 1 μ M dexamethasone (Cat: D4902) and 5 μ g/ml insulin (Cat: I9278). Cells were treated with 1 μ M Rosiglitazone or 1 μ M SR11023 from the initial day of differentiation. After incubation for six days, cells were harvested for RNA extraction or stained with Oil Red dye (Cat: O0625) to visualize lipid droplets

Cell-based transactivation assay.—HEK293T cells were co-transfected in batch by adding 4.5 μ g Gal4-PPAR γ -LBD, 4.5 μ g GAL4-PPAR α -LBD, or 4.5 μ g GAL4-mPPAR α -LBD, and 4.5 μ gUAS-luciferase reporter. Transfections were conducted using the X-treme Gene 9 transfection reagent (Cat: 6365779001), using manufacturer's protocol. After 18-h incubation at 37 °C, transfected cells were plated in triplicates in white 384-well plates (Perkin Elmer) at a density of 10,000 cells per well. After re-plating, cells were treated with either DMSO only or the indicated compounds in increasing doses from 2 pM–10 μ M. After 18-h incubation, treated cells were developed with Brite Lite Plus (Perkin Elmer) and read in 384-well Luminescence Perkin Elmer EnVision Multilabel plate reader. Graphs were plotted as fold change of treated cells over DMSO-treated control cells.

PPAR γ Binding Assays.—LanthaScreen TR-FRET PPAR γ competitive binding assay (Cat:PV4893) was performed according to the manufacturer's protocol. A mixture of 5 nM PPAR γ ligand binding domain (GST-PPAR γ -LBD, Cat:PV4545) or PPAR α ligand binding domain (GST-PPAR α -LBD, Cat:PV4691), 5 μ M Tb-GST-antibody (Cat:PV3550), 5 nM Fluormone Pan-PPAR Green (Cat:PV4896), and serial dilutions of compound beginning at 10 μ M downwards was added to wells of black 384-well low-volume plates (Greiner) to a total volume of 18 μ l. All dilutions were made in TR-FRET PPAR assay buffer. DMSO at 2% final concentration was used as a no-ligand control. Experiments were performed in triplicate and incubated for 2h in the dark before analysis in Perkin Elmer ViewLux ultra HTS microplate reader. The FRET signal was measured by excitation at 340 nm and emission at 520 nm for fluorescein and 490 nm for terbium. The fold change over DMSO was calculated by 520 nm/490 nm ratio. Graphs were plotted in GraphPad Prism as fold change of FRET signal for each compound over DMSO-only control. IC₅₀s were determined from GraphPad Prism software.

Quantitative PCR.—Total RNA was extracted from tissues using Qiazol reagent (Cat: 79306) and RNeasy Mini Kit (Cat:74104). Subsequently, cDNA was generated using High Capacity Reverse Transcription Kit (Applied Biosystems, Cat: 4368814). Quantitative PCR reactions were performed with SYBR green fluorescent dye (Cat: 1725271) using a 7900HT Fast Real-Time qPCR. Relative mRNA expression was determined by the $-C_t$ method normalized to Tbp levels. The sequences of primers used in this study are found in Table S1.

In vitro kinase assay.—Active Cdk5/p35 kinase (Cat:14–477) were purchased from Millipore. In vitro CDK kinase assay was performed using the HTScan CDK/Cyc kinase assay kit (Cat:7519) according to the manufacturer's instructions (Cell Signaling Technology). Briefly, 1 μ g of immuno-purified WT PPAR γ were incubated with active CDK kinase in kinase assay buffer (25 mM Tris-HCl pH 7.5, 5 mM β -glycerophosphate, 2 mM dithiothreitol (DTT), 0.1 mM Na₃VO₄, 10 mM MgCl₂) containing 20 μ M ATP for 15 min at 30 °C. SR11023 was pre-incubated with substrates for 30 min before performing assay. Phosphorylation of substrates after SDS–PAGE was analysed with anti-CDK substrate antibody to detect phospho-Ser in a K/R-S-P-K/R motif, which is the consensus motif for Cdk substrate proteins (Cell Signaling Technology).

Molecular docking.—The ICM Molsoft suite (Abagyan and Totrov, 1994) was used to dock compound SR11023 into the PPAR γ LBD structure. PDB 3FUR with ligands and water removed was used as the starting model for docking. The PPAR γ LBD structure was prepared for docking by protonation, deletion of water molecules, and energy minimization by means of the ICM force field and distance dependent dielectric potential with an RMS gradient of 0.1. PocketFinder within ICM was used to define the ligand binding pocket and was consistent with previously published X-ray structures. Default settings within the ICM docking module were used with a rectangular box centered at the LBD with a grid spacing of 0.5 Å. The top ranked docking for SR11023 was chosen for interpretation, as the conformations were very consistent among all the top scored dockings.

BS3 mediated crosslinking mass spectrometry.—PPAR γ LBD (10 μ M) (Hughes et al., 2012a) or PPAR γ /RXR α heterodimer (Kojetin et al., 2015) complex with or without PPAR γ ligand (10-fold excess)/SRC1–2/NCOR1–3/SMRT-2 (all peptides were 5-fold excess to protein) were incubated with BS3 (50-fold molar excess) (Cat:21580) for 1hr. Reaction was quenched with 50 mM Tris buffer and protein samples were overnight digested with trypsin (trypsin: protein ratio = 1:20, w/w) (Cat:V5111) and sequentially overnight digested with chymotrypsin (chymotrypsin: protein ratio = 1:20, w/w) (Cat:V1061) prior to analysis by LC-MS/MS. We specifically used chymotrypsin to introduce a specific cleavage between Tyrosine473 and Lysine474 for identification of a shorter peptide K474DLY, which resides on the C-terminus of AF2 α -helix. The lysine residue has a flexible 6 Å side chain while BS3 has an 8-atom spacer arm (11.4 Å). As a result, K474 could be cross-linked by BS3 to proximal lysine residues within the PPAR γ LBD (within the distance of 24 Å). Plink2 software was used to analyze and identify the XL-peptides (Yang et al., 2012). The parameters for pLink2 search were as follows: three missed cleavage sites for trypsin/ chymotrypsin per chain; peptide length 4 – 100 amino acid; pLink2 search results were filtered by requiring precursor tolerance (\pm 10 p.p.m.) and fragment tolerance (\pm 15 p.p.m.)

and FDR below 5% was required for all identified XL-MS peaks. The ion intensities and peak areas of the crosslinked peptides from different experimental conditions were manually calculated and compared. The highest peak intensity across all indicated experimental conditions within each bar plot panel was normalized as 100% and other peak abundances were scaled accordingly. Experiments were triplicated. Statistical summary was from a two-way ANOVA between indicated pairwise experiment (*** = $p < 0.001$; ** = $p < 0.01$; * = $p < 0.05$).

Hydrogen-deuterium exchange (HDX) detected by mass spectrometry.—

Solution-phase amide HDX experiments were carried out with a fully automated system (CTC HTS PAL, LEAP Technologies, Carrboro, NC; housed inside a 4°C cabinet) as described previously with slight modifications (Chalmers et al., 2006).

Peptide Identification: Peptides were identified using tandem MS (MS/MS) experiments performed with either a LTQ Orbitrap XL with ETD or a Q Exactive (Thermo Fisher Scientific, San Jose, CA) over a 70-min gradient. Product ion spectra were acquired in a data-dependent mode and the five most abundant ions were selected for the product ion analysis per scan event. The MS/MS *.raw data files were converted to *.mgf files and then submitted to MASCOT (version 2.3 Matrix Science, London, UK) for peptide identification. The maximum number of missed cleavages was set at 4 with the mass tolerance for precursor ions ± 0.6 Da and for fragment ions ± 8 ppm. Oxidation to methionine was selected for variable modification. Pepsin was used for digestion and no specific enzyme was selected in the MASCOT during the search. Peptides included in the peptide set used for HDX detection had a MASCOT score of 20 or greater. The MS/MS MASCOT search was also performed against a decoy (reverse) sequence and false positives were ruled out if they did not pass a 1% false discovery rate. The MS/MS spectra of all the peptide ions from the MASCOT search were further manually inspected and only the unique charged ions with the highest MASCOT score were included in HDX peptide set.

HDX-MS analysis: 10 μ M of the *apo* protein was mixed with 1:10 molar excess of ligand and incubated for 2 hours at 4°C for complex formation before subjecting them to HDX analysis. For the differential HDX experiments, 5 μ l of either the *apo* or the liganded protein complex were mixed with 20 μ l of D₂O-containing HDX buffer (50 mM Tris, pH 8.0, 150 mM NaCl, and 2 mM DTT) and incubated at 4°C for 0s, 10s, 30s, 60s, 300s, 900s or 3,600s. Following on-exchange, unwanted forward- or back-exchange was minimized and the protein was denatured by the addition of 25 μ l of a quench solution (1% v/v TFA in 3 M urea and 50 mM TCEP). Samples were then immediately passed through an immobilized pepsin column (prepared in house) (Busby et al., 2007) at 50 μ l min⁻¹ (0.1% v/v TFA, 15°C) and the resulting peptides were trapped and desalted on a 1.0 mm \times 10 mm C₈ trap column (Hypersil Gold, Thermo Fisher, Grand Island, NY). The bound peptides were then gradient-eluted (5–50% CH₃CN v/v and 0.3% v/v formic acid) across a 1.0 mm \times 50 mm C₁₈ separation column (Hypersil Gold, Thermo Fisher, Grand Island, NY) for 6 min. Sample handling and peptide separation were conducted at 4°C. The eluted peptides were then subjected to electrospray ionization directly coupled to a high resolution Orbitrap mass spectrometer (LTQ Orbitrap XL with ETD, Q Exactive, or Exactive, Thermo Fisher

Scientific, San Jose, CA). Each HDX experiment was carried out in triplicate with a single preparation of each protein-ligand complex. The intensity weighted mean m/z centroid value of each peptide envelope was calculated and subsequently converted into a percentage of deuterium incorporation. This is accomplished by determining the observed averages of the undeuterated and fully deuterated spectra using the conventional formula described elsewhere (Zhang and Smith, 1993). In the absence of a fully deuterated control, 100% deuterium incorporation was calculated theoretically, and corrections for back-exchange were made on the basis of an estimated 70% deuterium recovery and accounting for 79.9% final deuterium concentration in the sample (1:5 dilution in D_2O HDX buffer). Statistical significance for the differential HDX data is determined by an unpaired t-test for each time point, a procedure that is integrated into the HDX Workbench software (Pascal et al., 2012).

Data Rendering: The HDX data from all overlapping peptides were consolidated to individual amino acid values using a residue averaging approach. Briefly, for each residue, the deuterium incorporation values and peptide lengths from all overlapping peptides were assembled. A weighting function was applied in which shorter peptides were weighted more heavily and longer peptides were weighted less. Each of the weighted deuterium incorporation values were then averaged incorporating this weighting function to produce a single value for each amino acid. The initial two residues of each peptide, as well as prolines, were omitted from the calculations. This approach is similar to that previously described (Keppel and Weis, 2015).

NR box peptide recruitment assay.—A TR-FRET-based interaction assay was used. Tb-anti-His antibody (7.5 nM; Cat:PV5863) and a gradient of ligand concentrations were incubated in complete TR-FRET Nuclear receptor buffer F (Cat: PV4547) containing 7.5 nM purified His-PPAR γ 2 for 1 hr at room temperature. 450nM FITC-labeled peptides p300 (sequence: ASKHKQLSELLRSGSS), SMRT-2 (TNMGLEAIIRKALMGKYDQWEE), SRC1-2 (LTERHKILHRLQEGSPSD), and NCOR1-3 (ASNLGLEDIIRKALMGSD) were added and incubated for additional two hrs at room temperature (in dark). The FRET signal was measured by excitation at 340 nm and emission at 520 nm for fluorescein and 490 nm for terbium in Perkin Elmer ViewLux ultra HTS microplate reader. The fold change over DMSO was calculated by 520 nm/490 nm ratio. Graphs were plotted in GraphPad Prism as fold change of FRET signal for each compound over DMSO-only control.

mRNA-seq.—L1 cells RNA extraction protocol for RNA seq was derived from RNeasy Mini Kit (Cat:74106). Total RNA was quantified using the Qubit 2.0 Fluorometer (Invitrogen, Carlsbad, CA) and run on the Agilent 2100 Bioanalyzer (Agilent Technologies, Santa Clara, CA) for quality assessment. If the RNA profile is good quality with RNA Integrity Number (RIN) > 8.0, the samples are continued for processing. A RNase-free working environment is maintained and RNase-free tips, Eppendorf tubes and plates are utilized for the subsequent steps. Messenger RNA is selectively isolated from total RNA (typically 100–300ng input) using poly-T oligos attached to magnetic beads according to the TruSeq stranded mRNA sample prep protocol (Cat:RS-122–2101, Illumina, San Diego, CA). The enriched mRNA samples are chemically fragmented in a buffer containing divalent cations and heating at 94°C for 8 minutes. The fragmented RNA is random hexamer primed

and reverse transcribed to generate the first strand cDNA. The second strand is synthesized after removing the RNA template and incorporating dUTP in place of dTTP. The incorporation of dUTP quenches the second strand during the PCR amplification step later and therefore the strand information is preserved. The ds cDNA is then end repaired and adenylated at their 3' ends. A corresponding 'T' nucleotide on the adaptors is utilized for ligating the adaptor sequences to the ds cDNA. The adaptor ligated DNA is purified using magnetic Ampure XP beads and PCR amplified using 13 cycles to generate the final libraries. The final libraries are size selected and purified using 1.0 x Ampure XP beads to remove any primer dimers. The final library size is typically 200–600bp with insert sizes ranging from 80–450bp. The final libraries are validated by the bioanalyzer DNA chips, normalized to 1nM, pooled equally and loaded onto the NextSeq 500 flow cell at 1.8pM final concentration and sequenced using 2 × 75bp paired-end chemistry. On average, we generate 20–22 million reads pass filter (base quality score >Q30 suggesting less than 1 error in 1000bp).

NMR spectroscopy.—Two-dimensional (2D) [¹H, ¹⁵N]-transverse relaxation optimized spectroscopy (TROSY)-heteronuclear single quantum correlation (HSQC) data were collected at 298K using a Bruker 700 Mhz NMR instrument equipped with a QCI cryoprobe. Samples contained approximately 200 μM protein in a NMR buffer containing 50 mM potassium phosphate (pH 7.4), 20 mM potassium chloride, 1 mM TCEP, and 10% D₂O; with or without 2 equivalents NCOR1–3 or SMRT2 peptide, or with or without 2 equivalents of rosiglitazone, MRL24, or SR11023. Data were processed and analyzed using Topspin 3.0 (Bruker) and NMRViewJ (OneMoon Scientific, Inc.) (Johnson, 2004). NMR analysis was limited to well resolved peaks for residues with chemical shift values similar to PPAR γ bound to rosiglitazone (BMRB entry 17975) (Hughes et al., 2012b) using the minimum chemical shift procedure (Williamson, 2013).

Fluorescence polarization coregulatory binding assay.—His-PPAR γ LBD was prepared by serial dilution in assay buffer (50 mM potassium phosphate, 20 mM potassium chloride, 1 mM TCEP, 0.01% Tween 20, pH 7.4) and plated in black 384-well plates (Greiner) with peptides (100 nM final concentration) derived from the SMRT2 corepressor (TRAP220–2; residues 638–656; TNMGLEAIIRKALMGKYDQWEE) or the NCoR corepressor (NCoR-D3; residues 2256–2278; TITAANFIDVIITRQIASDK) containing a N-terminal FITC label with a six-carbon linker (Ahx). The plate was incubated at 4 °C for 2 hr and FP measured on a Spectramax M5e multimode plate reader at 485 nm excitation and 538 nm emission wavelengths. Data were analyzed using GraphPad Prism (FP signal vs. ligand concentration) and fit to one-site binding equation

QUANTIFICATION AND STATISTICAL ANALYSIS

HDX-MS analysis

Data Statistics: Deuterium uptake for each peptide is calculated as the average of % D for all on-exchange time points and the difference in average %D values between the *apo* and ligand bound samples is presented as a heat map with a color code given at the bottom of the Figure (warm colors for deprotection and cool colors for protection). Peptides are colored by the software automatically to display significant differences, determined either by a >5%

difference (less or more protection) in average deuterium uptake between the two states, or by using the results of unpaired t-tests at each time point (p-value < 0.05 for any two time points or a p-value < 0.01 for any single time point). Peptides with non-significant changes between the two states are colored grey. The exchange at the first two residues for any given peptide is not colored. Each peptide bar in the heat map view displays the average %D values, associated standard deviation, and the charge state. Additionally, overlapping peptides with a similar protection trend covering the same region are used to rule out data ambiguity.

Fluorescence polarization coregulatory binding assay/ NR box peptide recruitment assay/PPAR γ Binding Assays. Results are expressed as mean \pm SEM. The significance of differences between groups was evaluated by one-way analysis of variance (ANOVA) followed by a Dunnett's test for multiple comparisons, or Student's t-test with or without Bonferroni's correction. Analyses were done with GraphPad Prism software (GraphPad).

Data and Software Availability

The mass spec data have been deposited to the ProteomeXchange Consortium via the PRIDE (Vizcaino et al., 2016) partner repository with the accession number: PXD010222. HDX-MS data have been deposited to Figshare (<https://figshare.com/s/d9fe41df3e945828e548>). HDX data was processed by HDX Workbench (Pascal et al., 2012). XL-MS data was processed by plink2 (Yang et al., 2012).

Supplementary Material

Refer to Web version on PubMed Central for supplementary material.

ACKNOWLEDGEMENTS

This work was supported from the National Institutes of Health; NIH grants DK DK105825 (PI: P.R.G.), DK101871 (PI: D.J.K.), The Landenberger Foundation (J.Z.) and the Klorfine Family Fellowship (C.A.C.).

REFERENCES

- Abagyan R, and Totrov M (1994). Biased probability Monte Carlo conformational searches and electrostatic calculations for peptides and proteins. *J Mol Biol* 235, 983–1002. [PubMed: 8289329]
- Acton JJ, 3rd, Akiyama TE, Chang CH, Colwell L, Debenham S, Doebber T, Einstein M, Liu K, McCann ME, Moller DE, et al. (2009). Discovery of (2R)-2-(3-{3-[(4-Methoxyphenyl)carbonyl]-2-methyl-6-(trifluoromethoxy)-1H-indol-1-yl}phenoxy)butanoic acid (MK-0533): a novel selective peroxisome proliferator-activated receptor gamma modulator for the treatment of type 2 diabetes mellitus with a reduced potential to increase plasma and extracellular fluid volume. *Journal of medicinal chemistry* 52, 3846–3854. [PubMed: 19507861]
- Acton JJ, 3rd, Black RM, Jones AB, Moller DE, Colwell L, Doebber TW, Macnaul KL, Berger J, and Wood HB (2005). Benzoyl 2-methyl indoles as selective PPARgamma modulators. *Bioorg Med Chem Lett* 15, 357–362. [PubMed: 15603954]
- Asteian A, Blayo AL, He Y, Koenig M, Shin Y, Kuruvilla DS, Corzo CA, Cameron MD, Lin L, Ruiz C, et al. (2015). Design, Synthesis, and Biological Evaluation of Indole Biphenylcarboxylic Acids as PPARgamma Antagonists. *ACS Med Chem Lett* 6, 998–1003. [PubMed: 26396687]
- Banks AS, McAllister FE, Camporez JP, Zushin PJ, Jurczak MJ, Laznik-Bogoslavski D, Shulman GI, Gygi SP, and Spiegelman BM (2015). An ERK/Cdk5 axis controls the diabetogenic actions of PPARgamma. *Nature* 517, 391–395. [PubMed: 25409143]

- Bruning JB, Chalmers MJ, Prasad S, Busby SA, Kamenecka TM, He Y, Nettles KW, and Griffin PR (2007). Partial agonists activate PPAR γ using a helix 12 independent mechanism. *Structure* 15, 1258–1271. [PubMed: 17937915]
- Busby SA, Chalmers MJ, and Griffin PR (2007). Improving digestion efficiency under H/D exchange conditions with activated pepsinogen coupled columns. *Int J Mass Spectrom* 259, 130–139.
- Chalmers MJ, Busby SA, Pascal BD, He Y, Hendrickson CL, Marshall AG, and Griffin PR (2006). Probing protein ligand interactions by automated hydrogen/deuterium exchange mass spectrometry. *Analytical chemistry* 78, 1005–1014. [PubMed: 16478090]
- Chen ZA, Jawhari A, Fischer L, Buchen C, Tahir S, Kamenski T, Rasmussen M, Lariviere L, Bukowski-Wills JC, Nilges M, et al. (2010). Architecture of the RNA polymerase II-TFIIF complex revealed by cross-linking and mass spectrometry. *The EMBO journal* 29, 717–726. [PubMed: 20094031]
- Choi JH, Banks AS, Estall JL, Kajimura S, Bostrom P, Laznik D, Ruas JL, Chalmers MJ, Kamenecka TM, Bluher M, et al. (2010). Anti-diabetic drugs inhibit obesity-linked phosphorylation of PPAR γ by Cdk5. *Nature* 466, 451–456. [PubMed: 20651683]
- Choi JH, Banks AS, Kamenecka TM, Busby SA, Chalmers MJ, Kumar N, Kuruvilla DS, Shin Y, He Y, Bruning JB, et al. (2011). Antidiabetic actions of a non-agonist PPAR γ ligand blocking Cdk5-mediated phosphorylation. *Nature* 477, 477–481. [PubMed: 21892191]
- Fischer L, Chen ZA, and Rappsilber J (2013). Quantitative cross-linking/mass spectrometry using isotope-labelled cross-linkers. *J Proteomics* 88, 120–128. [PubMed: 23541715]
- Heldring N, Pike A, Andersson S, Matthews J, Cheng G, Hartman J, Tujague M, Strom A, Treuter E, Warner M, et al. (2007). Estrogen receptors: How do they signal and what are their targets. *Physiological reviews* 87, 905–931. [PubMed: 17615392]
- Horlein AJ, Naar AM, Heinzl T, Torchia J, Gloss B, Kurokawa R, Ryan A, Kamei Y, Soderstrom M, Glass CK, et al. (1995). Ligand-independent repression by the thyroid hormone receptor mediated by a nuclear receptor co-repressor. *Nature* 377, 397–404. [PubMed: 7566114]
- Hu X, and Lazar MA (1999). The CoRNR motif controls the recruitment of corepressors by nuclear hormone receptors. *Nature* 402, 93–96. [PubMed: 10573424]
- Hughes TS, Chalmers MJ, Novick S, Kuruvilla DS, Chang MR, Kamenecka TM, Rance M, Johnson BA, Burris TP, Griffin PR, et al. (2012a). Ligand and receptor dynamics contribute to the mechanism of graded PPAR γ agonism. *Structure* 20, 139–150. [PubMed: 22244763]
- Hughes TS, Chalmers MJ, Novick S, Kuruvilla DS, Chang MR, Kamenecka TM, Rance M, Johnson BA, Burris TP, Griffin PR, et al. (2012b). Ligand and receptor dynamics contribute to the mechanism of graded PPAR γ agonism. *Structure* 20, 139–150. [PubMed: 22244763]
- Johnson BA (2004). Using NMRView to visualize and analyze the NMR spectra of macromolecules. *Methods Mol Biol* 278, 313–352. [PubMed: 15318002]
- Keppel TR, and Weis DD (2015). Mapping residual structure in intrinsically disordered proteins at residue resolution using millisecond hydrogen/deuterium exchange and residue averaging. *Journal of the American Society for Mass Spectrometry* 26, 547–554. [PubMed: 25481641]
- Kintscher U, and Law RE (2005). PPAR γ -mediated insulin sensitization: the importance of fat versus muscle. *Am J Physiol Endocrinol Metab* 288, E287–291. [PubMed: 15637349]
- Knutson BA, Luo J, Ranish J, and Hahn S (2014). Architecture of the *Saccharomyces cerevisiae* RNA polymerase I Core Factor complex. *Nature structural & molecular biology* 21, 810–816.
- Kojetin DJ, Matta-Camacho E, Hughes TS, Srinivasan S, Nwachukwu JC, Cavett V, Nowak J, Chalmers MJ, Marciano DP, Kamenecka TM, et al. (2015). Structural mechanism for signal transduction in RXR nuclear receptor heterodimers. *Nature communications* 6, 8013.
- Kung J, and Henry RR (2012). Thiazolidinedione safety. *Expert opinion on drug safety* 11, 565–579. [PubMed: 22616948]
- le Maire A, Teyssier C, Erb C, Grimaldi M, Alvarez S, de Lera AR, Balaguer P, Gronemeyer H, Royer CA, Germain P, et al. (2010). A unique secondary-structure switch controls constitutive gene repression by retinoic acid receptor. *Nature structural & molecular biology* 17, 801–807.
- Liu K, Black RM, Acton JJ, 3rd, Mosley R, Debenham S, Abola R, Yang M, Tschirret-Guth R, Colwell L, Liu C, et al. (2005). Selective PPAR γ modulators with improved pharmacological profiles. *Bioorganic & medicinal chemistry letters* 15, 2437–2440. [PubMed: 15863293]

- Marciano DP, Kuruvilla DS, Boregowda SV, Asteian A, Hughes TS, Garcia-Ordenez R, Corzo CA, Khan TM, Novick SJ, Park H, et al. (2015). Pharmacological repression of PPAR gamma promotes osteogenesis. *Nature communications* 6.
- Mayans L (2015). Metabolic Syndrome: Insulin Resistance and Prediabetes. *FP Essent* 435, 11–16. [PubMed: 26280340]
- Merkley ED, Rysavy S, Kahraman A, Hafen RP, Daggett V, and Adkins JN (2014). Distance restraints from crosslinking mass spectrometry: mining a molecular dynamics simulation database to evaluate lysine-lysine distances. *Protein Sci* 23, 747–759. [PubMed: 24639379]
- Minoura H, Takeshita S, Ita M, Hirosumi J, Mabuchi M, Kawamura I, Nakajima S, Nakayama O, Kayakiri H, Oku T, et al. (2004). Pharmacological characteristics of a novel nonthiazolidinedione insulin sensitizer, FK614. *European journal of pharmacology* 494, 273–281. [PubMed: 15212984]
- Muller F, Fischer L, Chen ZA, Auchynnikava T, and Rappsilber J (2018). On the Reproducibility of Label-Free Quantitative Cross-Linking/Mass Spectrometry. *J Am Soc Mass Spectrom* 29, 405–412. [PubMed: 29256016]
- Nagy L, Kao HY, Love JD, Li C, Banayo E, Gooch JT, Krishna V, Chatterjee K, Evans RM, and Schwabe JW (1999). Mechanism of corepressor binding and release from nuclear hormone receptors. *Genes & development* 13, 3209–3216. [PubMed: 10617570]
- Nolte RT, Wisely GB, Westin S, Cobb JE, Lambert MH, Kurokawa R, Rosenfeld MG, Willson TM, Glass CK, and Milburn MV (1998). Ligand binding and co-activator assembly of the peroxisome proliferator-activated receptor-gamma. *Nature* 395, 137–143. [PubMed: 9744270]
- Pascal BD, Willis S, Lauer JL, Landgraf RR, West GM, Marciano D, Novick S, Goswami D, Chalmers MJ, and Griffin PR (2012). HDX workbench: software for the analysis of H/D exchange MS data. *J Am Soc Mass Spectrom* 23, 1512–1521. [PubMed: 22692830]
- Rizos CV, Elisaf MS, Mikhailidis DP, and Liberopoulos EN (2009). How safe is the use of thiazolidinediones in clinical practice? *Expert Opin Drug Saf* 8, 15–32. [PubMed: 19236215]
- Rubenstrunk A, Hanf R, Hum DW, Fruchart JC, and Staels B (2007). Safety issues and prospects for future generations of PPAR modulators. *Biochimica et biophysica acta* 1771, 1065–1081. [PubMed: 17428730]
- Schmidt C, and Robinson CV (2014). A comparative cross-linking strategy to probe conformational changes in protein complexes. *Nat Protoc* 9, 2224–2236. [PubMed: 25144272]
- Shi L, Zhao Y, Szymanski K, Yau L, and Fonseca V (2011). Impact of thiazolidinedione safety warnings on medication use patterns and glycemic control among veterans with diabetes mellitus. *Journal of diabetes and its complications* 25, 143–150. [PubMed: 20708416]
- Stechschulte LA, Czernik PJ, Rotter ZC, Tausif FN, Corzo CA, Marciano DP, Asteian A, Zheng J, Bruning JB, Kamenecka TM, et al. (2016). PPARγ Post-translational Modifications Regulate Bone Formation and Bone Resorption. *EBioMedicine* 10, 174–184. [PubMed: 27422345]
- Sugii S, Olson P, Sears DD, Saberi M, Atkins AR, Barish GD, Hong SH, Castro GL, Yin YQ, Nelson MC, et al. (2009). PPARγ activation in adipocytes is sufficient for systemic insulin sensitization. *Proc Natl Acad Sci U S A* 106, 22504–22509. [PubMed: 20018750]
- Vizcaino JA, Csordas A, Del-Toro N, Dianas JA, Griss J, Lavidas I, Mayer G, Perez-Riverol Y, Reisinger F, Ternent T, et al. (2016). 2016 update of the PRIDE database and its related tools. *Nucleic Acids Res* 44, 11033. [PubMed: 27683222]
- Williamson MP (2013). Using chemical shift perturbation to characterise ligand binding. *Prog Nucl Magn Reson Spectrosc* 73, 1–16. [PubMed: 23962882]
- Wright MB, Bortolini M, Tadayyon M, and Bopst M (2014). Minireview: Challenges and opportunities in development of PPAR agonists. *Molecular endocrinology* 28, 1756–1768. [PubMed: 25148456]
- Wu B, Peisley A, Richards C, Yao H, Zeng X, Lin C, Chu F, Walz T, and Hur S (2013). Structural basis for dsRNA recognition, filament formation, and antiviral signal activation by MDA5. *Cell* 152, 276–289. [PubMed: 23273991]
- Xu HE, Stanley TB, Montana VG, Lambert MH, Shearer BG, Cobb JE, McKee DD, Galardi CM, Plunket KD, Nolte RT, et al. (2002a). Structural basis for antagonist-mediated recruitment of nuclear co-repressors by PPAR alpha. *Nature* 415, 813–817. [PubMed: 11845213]

- Xu HE, Stanley TB, Montana VG, Lambert MH, Shearer BG, Cobb JE, McKee DD, Galardi CM, Plunket KD, Nolte RT, et al. (2002b). Structural basis for antagonist-mediated recruitment of nuclear co-repressors by PPARalpha. *Nature* 415, 813–817. [PubMed: 11845213]
- Yang B, Wu YJ, Zhu M, Fan SB, Lin J, Zhang K, Li S, Chi H, Li YX, Chen HF, et al. (2012). Identification of cross-linked peptides from complex samples. *Nat Methods* 9, 904–906. [PubMed: 22772728]
- Zhang Z, and Smith DL (1993). Determination of amide hydrogen exchange by mass spectrometry: a new tool for protein structure elucidation. *Protein science : a publication of the Protein Society* 2, 522–531. [PubMed: 8390883]

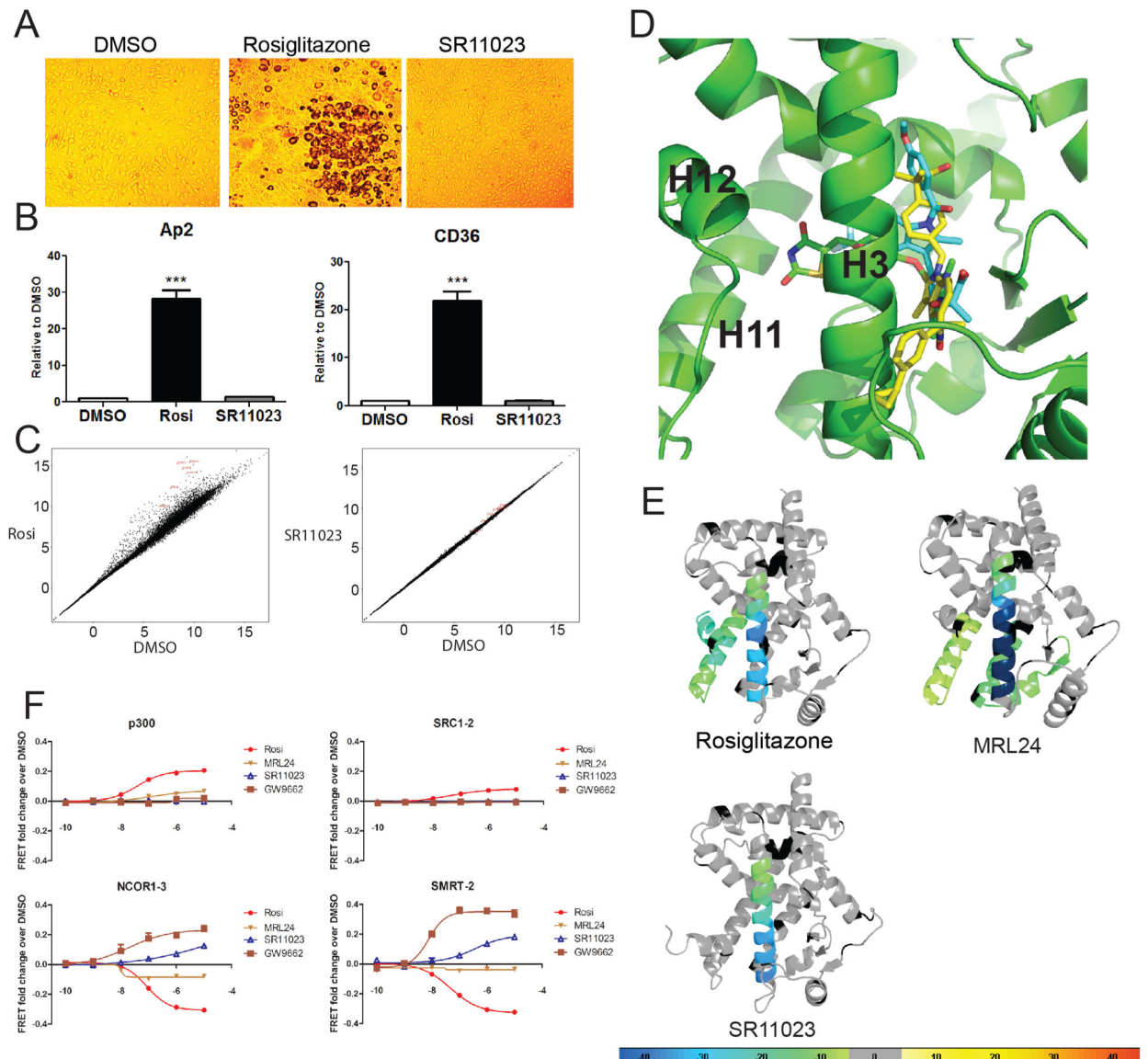


Figure 1. SR11023 functions as a non-agonist of PPAR γ .

(A) Oil red staining of differentiated 3T3-L1 adipocytes in the presence of Rosiglitazone or SR11023. (B) Expression of adipocyte genes in differentiated 3T3-L1 cells. Results are expressed as mean \pm SEM. (C) Linear plot of RNA-seq data of differential gene expression in 3T3-L1 cells induced by 6-day ligand treatments. (D) Superimposition of SR11023, MRL24 and Rosiglitazone within PPAR γ LBD. Top scoring *in silico* docking binding pose for SR11023 using chain A of PDB: 4R06 (atomic coordinates specific for PPAR γ crystal structure from the Protein Structure Database). (E) Differential consolidation HDX data are mapped onto the PPAR γ LBD structure, as shown by representation of altered conformational dynamics of receptor upon binding to Rosi, MRL24 and SR11023. Percentages of deuterium differences are color-coded according to the smooth color gradient key in the bottom. (F) TR-FRET analysis of His-PPAR γ interaction with FITC-labeled peptides representative of NR binding motifs from either transcriptional co-activators (p300

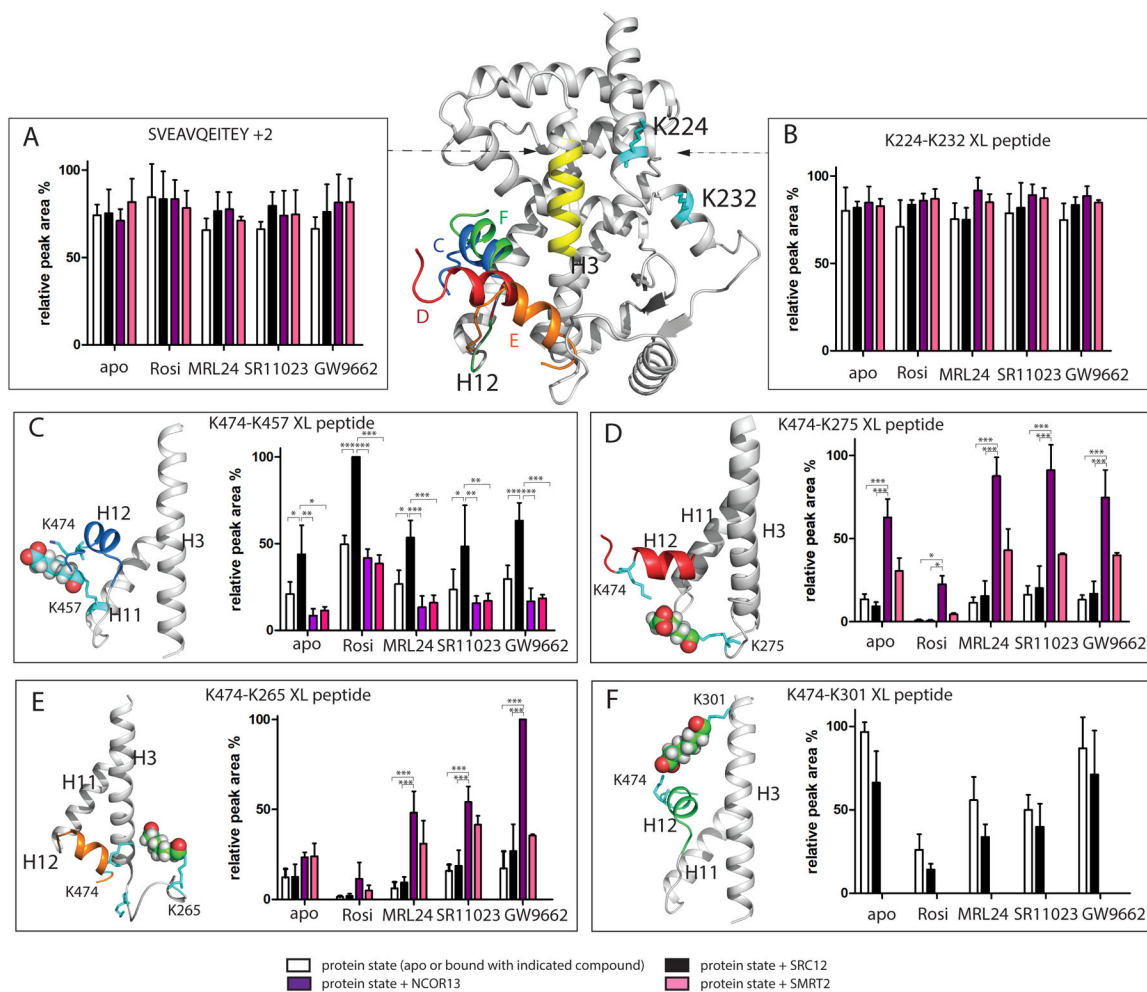
and SRC1-2) or co-repressors (NCOR1-3 and SMRT-2) in the presence of increasing concentrations of Rosi, MRL24 and SR11023. GW9662, a potent antagonist of PPAR γ , is used as a control ligand. See also Figure S1 and Figure S2A and S2B.

Author Manuscript

Author Manuscript

Author Manuscript

Author Manuscript



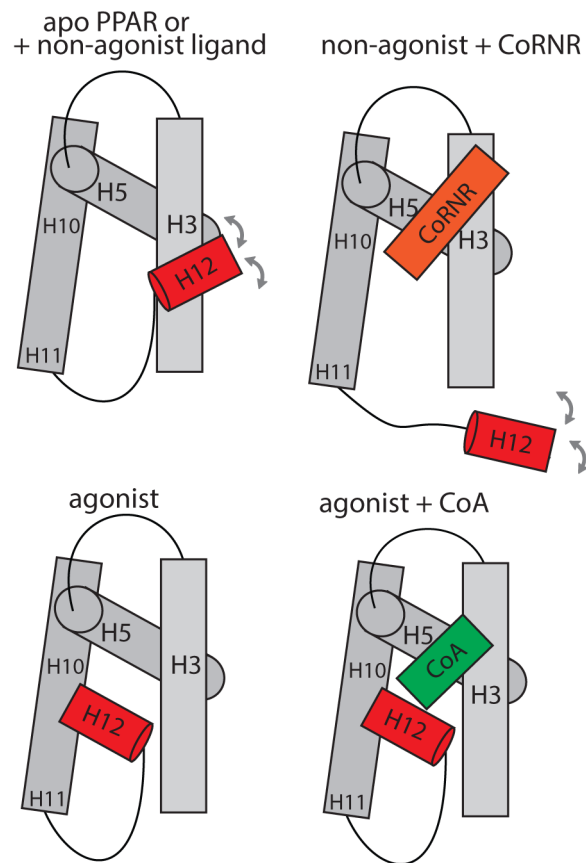


Figure 3. PPAR γ H12 mobility based on XL-MS observation.

In the apo or inverse agonist bound state, H12 adopts an ensemble of multiple populations swing around H3. Binding of inverse agonist to PPAR γ further stabilize the interaction with CoRNR, which displaces H12 from folding back to agonist position. In contrast, agonist binding directly stabilize H12 into an agonist position, which forms AF2 surface with H3 and H5 for CoA binding.

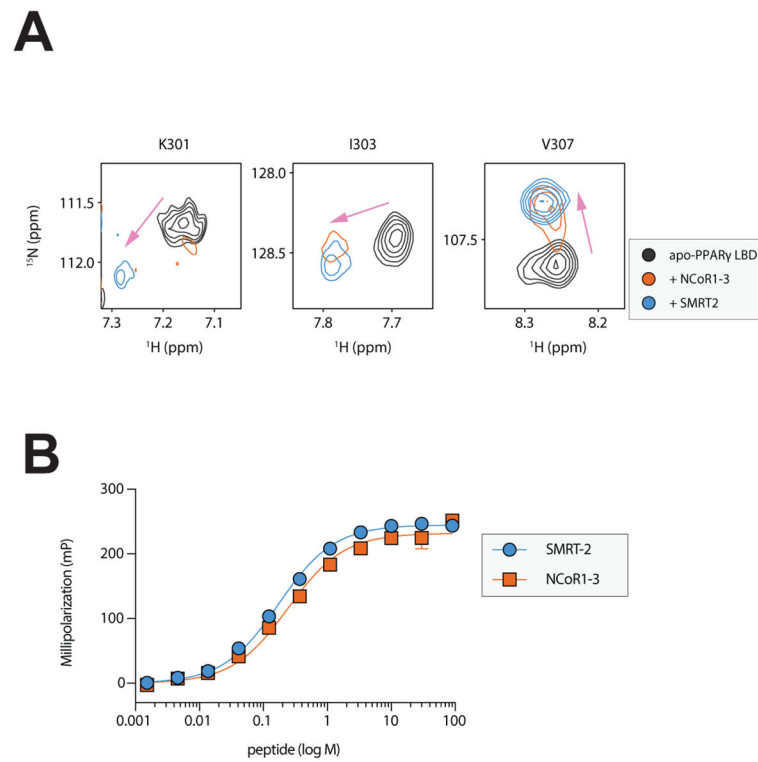
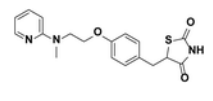
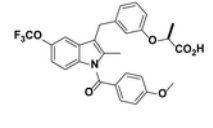
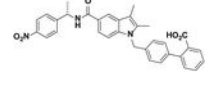
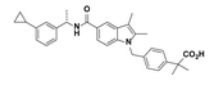


Figure 4. NMR chemical shift induced by co-repressor peptide

(A) Differential 2D [^1H , ^{15}N]-TROSY-HSQC NMR data comparing apo-PPAR γ without or with 2 equivalents of NCoR1-3 or SMRT2 corepressor peptide. (B) Fluorescence polarization assay data showing the affinity of PPAR γ for NCoR1-3 (240 nM) and SMRT2 (170 nM) are similar. Results are expressed as mean \pm SEM.

Table 1

Compound structures and characteristics

Compound	Chemical structures	IC ₅₀ ^a (nM) PPAR γ	EC ₅₀ ^a (nM), Max.Stim. PPAR γ Gal-4	EC ₅₀ ^a (nM) PPRE	EC ₅₀ ^a (μ M) PPAR α GAL-4	% inhibition p273- PPAR γ (2 μ M, 20 μ M)
Rosiglitazone		18	7.4, 100%	10	No activity	85, 100 (Choi et al., 2011)
MRL24		1	2, 21% (Acton et al., 2005)	NT	NT	More potent than Rosi to inhibit p273 (Choi et al., 2010)
SR1664		80	4501, 10% (Asteian et al., 2015)	No activity	8.6	90, 100 (Choi et al., 2011)
SR11023		108	2761, 10%	No activity	No activity	25, 77

^a% transactivation at 10 μ M; NT: not tested